Applied Physics A (2018) 124:663
https://doi.org/10.1007/s00339-018-2091-6

Applied Physics A
Materials Science & Processing

Dual functions of thiourea for solution combustion synthesis of ZnO/ZnS composite powders: fuel and sulphur source

Majid Zahiri[1] · Mahdi Shafiee Afarani[1] · Amir Masoud Arabi[2]

Received: 31 May 2018 / Accepted: 1 September 2018 / Published online: 5 September 2018

Abstract
In the present study, ZnO/ZnS composite powders were synthesized by one-step solution combustion method. Thiourea was used both as the combustion fuel and sulphur source. Oxidizer-to-fuel (O:F) ratios between 0.5 and 1 were chosen as the main synthesis parameter. Structure, microstructure, chemical composition, and photoluminescence properties of the powders were also investigated. X-ray diffraction patterns showed simultaneous functions of thiourea as combustion fuel and sulphur source. The relative concentration of ZnS to ZnO increased by O:F ratio. Fourier-transform infra-red spectroscopy spectra demonstrated some bands associated with the unwanted organic compounds in the final product in addition to Zn–O and Zn–S bonds. Furthermore, scanning electron microscope micrographs showed the presence of some gel-like regions located around highly agglomerated particles. Photoluminescence spectra also indicated strong emission peaks for O:F ratio of 0.5 due to significant crystal defects and lower crystallinity.

1 Introduction

Zinc oxide (ZnO) as a semiconductor with a wide bandgap (~3.3 eV) is used in many applications such as varistors, functional devices, thermoelectric materials, UV protection, photocatalysis, luminescence materials in LED, and superhydrophobic coatings due to its excellent physical and chemical properties [1–6]. Therefore, it can be widely used for information technology, bio-technology, and environmental technology as the next generation technologies.

Zinc sulfide is another important semiconductor compound which belongs to groups IIB–VIB and has a broad energy gap of about 3.68 eV [7, 8]. It has particular applications in optoelectronic devices [9], solar cells [10], and bioluminescent labels [11, 12]. Moreover, this pigment is used along with titanium dioxide as a UV-resistant pigment [13]. Zinc oxide–zinc sulfide composite may lead to a lower photoexcitation threshold energy than that of ZnO and ZnS, alone. It is due to the decreased recombination rate of electron–hole pairs by physically separated charge carriers [14, 15]. In addition, this composite may be used as a visible-light sensible material because of its oxy-sulfide nature [16]. There are numerous investigations on the synthesis of ZnO, ZnS, and ZnO/ZnS powder composites with different methods such as precipitation, co-precipitation, self-propagating high-temperature synthesis (SHS), volume combustion synthesis, sol–gel, and hydrothermal synthesis [17–23]. However, to the best of our knowledge, synthesis of ZnO/ZnS composite powder with solution combustion method is more than scarce. Solution combustion synthesis (SCS) method was selected because of its several advantages including easy-eco, rapid reaction using inexpensive starting materials [24].

The aim of the present study was the one-step synthesis of ZnO/ZnS nanocomposite via solution combustion method. Thiourea is used instead of routine fuels like citric acid and glycine, because not only it plays the role of combustion fuel, but also it provides the required sulphur for the formation of ZnS. In addition, the effects of oxidizer to fuel (O:F) ratios on the structure, chemical composition, microstructure, and photoluminescence properties of powders were studied.

✉ Mahdi Shafiee Afarani
majidzahiri.1992@yahoo.com; mshafiee@eng.usb.ac.ir

Amir Masoud Arabi
aarabi@acrc.ac.ac.ir

[1] Department of Materials Engineering, Faculty of Engineering, University of Sistan and Baluchestan, Zahedan, Iran

[2] Department of Inorganic Pigments and Glazes, Institute for Color Science and Technology (ICST), Tehran, Iran

2 Experimental

Zinc nitrate hexahydrate [Zn $(NO_3)_2 \cdot 6H_2O$, MERCK] was used as the starting material, while thiourea (CH_4N_2S, MERCK) was added both as the fuel and the sulphur source. Combustion reactions were performed based on propellant chemistry explained by Kingsley and Patil [25]. In this method, stoichiometric concentration of metal nitrate is calculated with respect to the total oxidizing and reducing values of oxidizer and fuel. If the ratio of total valences of oxidizer to fuel is equal to 1, it means that the stoichiometric condition and the maximum combustion intensity occur. Two sets of reactions during the dissolution of reactants, gel formation, ignition, and final combustion were considered as follows:

- Set 1: Reactions for the formation of ZnO [26].

  (i) Partial decomposition of thiourea during the solution transformation to the gel, and gradual increase of pH values from low acidic values to neutral and moderate basic conditions:

$$CS(NH_2)_2(\text{thiourea}) \rightarrow NH_4^+ + NSC^-. \quad (1)$$

  (ii) Substitution of a parallel reaction instead of Eq. 1:

$$OH^- + CS(NH_2)_2 \rightarrow SH^- + CO(NH_2)_2(\text{urea}). \quad (2)$$

  (iii) Combustion reaction of urea (as a product of reaction 2) and zinc nitrate based on the propellant chemistry:

$$Zn(NO_3)_2 + \Psi CO(NH_2)_2 \rightarrow ZnO + \Psi CO_2 + 2\Psi H_2O + \Psi N_2, \quad (3)$$

  where Ψ is the oxidizer to fuel ratio. In Eq. 3, calculated Ψ value is equal to $\frac{5}{3}$ as follows:

$$\Psi = \frac{\sum \text{Total valences of oxidizer}}{\sum \text{Total valences of fuel}} = \frac{\sum 2 - [(0 + 2 \times 3) \times 2]}{\sum 4 - 2 + [(0 + 2 \times 1) \times 2]} = \frac{5}{3}.$$

  It is shown that the O/F ratio is above 1 and the fuel-rich condition was occurred. Therefore, the progress of ignition depends on the excess amount of thiourea.

- Set 2: Reactions for the formation of ZnS [27].

  (a) Reaction of zinc nitrate and water to form zinc hydroxide due to decomposition of urea (Eq. 1) and consequently, the increase of pH value:

$$Zn(NO_3)_3 + H_2O \rightarrow Zn(OH)_2 + 2HNO_3. \quad (4)$$

  (b) Simultaneous reaction of thiourea with water to form hydrogen sulfide, ammonia, and carbon dioxide:

$$CS(NH_2)_2 + H_2O \rightarrow H_2S + NH_3 + CO_2. \quad (5)$$

  (c) Combination of reactions (4) and (5) to form ZnS as follows:

$$Zn(NO_3)_2 + H_2S \rightarrow ZnS + 2H_2O. \quad (6)$$

There is competition between the two sets of reactions, and both thermodynamic and kinetic aspects of the reactions can affect the final composition of ZnO/ZnS composite. It seems that the strength of reactions in set 1 is basically adjusted by O:F ratios. Therefore, O:F ratios up to stoichiometric amount can suppress quick progressive reactions toward ZnO structure. As a result, the competition leads to the nanocomposite structure.

As a typical procedure, an aqueous solution (0.5 M) was prepared by dissolution of 2.97 g zinc nitrate hexahydrate in 20 ml distilled water in a volumetric flask. Then, thiourea as the main fuel was added to the solution with different O:F ratios. The pH values were adjusted between 2 and 3 by adding nitric acid. The resultant mixture was agitated under magnetic stirring at 200 °C for 30 min until a thick white hydro-gel was obtained which was heated on a heater stirrer at 250 °C for 3 min until the combustion reaction was occurred. Structure and microstructure analyses of the samples were performed using XRD (Bruker, Advance D8) and scanning electron microscopy (SEM, KYKY 3900) techniques, respectively. Fourier transformed infra-red spectrometer (FTIR Bruker, Tensor II) was used for the molecular analysis of the samples. Photoluminescence (PL) spectra were obtained using a Perkin Elmer LS 55 Luminescence spectrometer with the exciting wavelength of 360 nm.

3 Results and discussion

XRD patterns of the samples synthesized with different O:F ratios are shown in Fig. 1. As illustrated, both ZnO (card no. 01-079-0207) and ZnS (card no. 00-001-1280) phases were formed in the sample synthesized at equal ratio of oxidizer to fuel (O:F = 1). No minor phases were observed. Narrow high-intensity peaks showed the formation of highly crystalline phases. It can be related to the considerable heat liberated from the combustion reaction that facilitated the

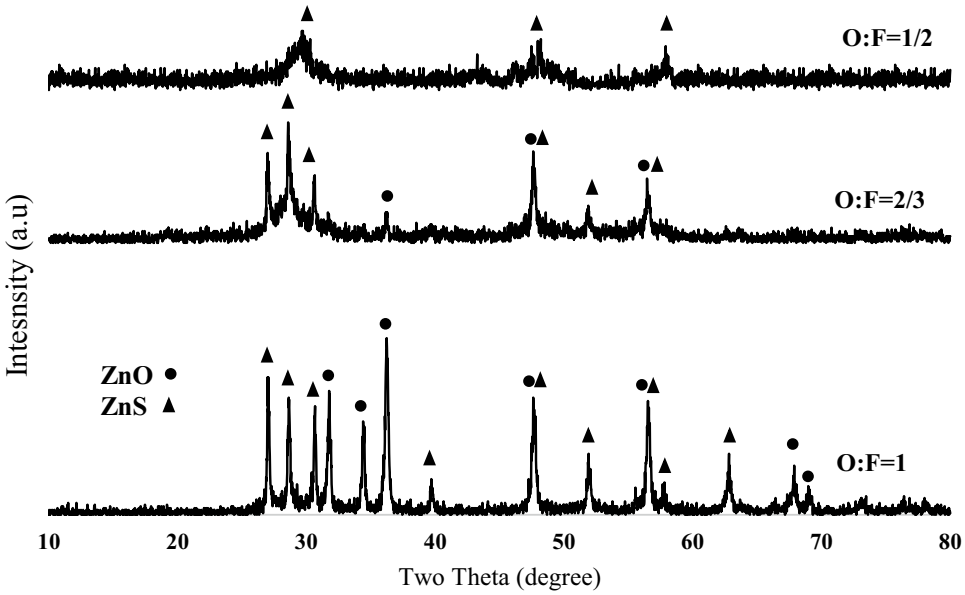

Fig. 1 XRD patterns of samples synthesized with O:F ratios of 1, 2/3, and 1/2

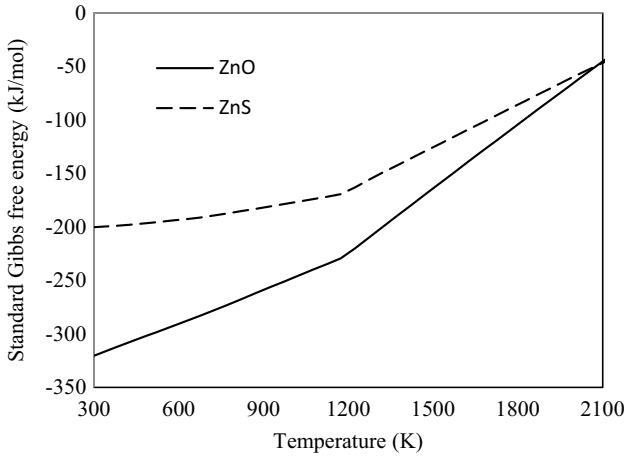

Fig. 2 Formation standard Gibbs free energy variation (ΔG^0) versus temperature for ZnO and ZnS

grain growth. Increase in the fuel content (O:F ratio of 0.66) caused the lack of sufficient oxygen for complete reaction between Zn and O. Therefore, combination of Zn and S led to the formation of ZnS as the predominant phase with minor amounts of ZnO. Further decrease of O:F ratio to 0.5 caused the broadening and weakening of the ZnS peaks as a result of nanoparticle formation.

To have a better understanding on the stability of ZnO and ZnS phases, the formation standard Gibbs free energy variation (ΔG^0) graphs versus temperature is drawn in Fig. 2 using data presented in [28] according to the following reactions:

$$Zn + 1/2O_2 \rightarrow ZnO \quad (7)$$

$$Zn + S \rightarrow ZnS. \quad (8)$$

As illustrated, ZnO has less Gibbs free energies than ZnS below 2000 K. Therefore, the ZnO phase is thermodynamically more stable than ZnS in the range of 300 – 2000 K. Therefore, there is more tendency for the formation of zinc oxide in the presence of sufficient oxidizer. Therefore, the increase of oxygen content (O:F ratio of 1) provides enough oxygen for the formation of ZnO. As a result, ZnO and ZnS phases are obtained.

Figure 3 shows FTIR spectra of samples synthesized with different O:F ratios. Since ZnO and ZnS have similar crystal structures and bonds' strengths, their FTIR bands are near to each other. The bands at 411–480 cm^{-1} are associated with Zn–O stretching bond [29]. The bands in the ranges of 1109–1128 cm^{-1} and 600–800 are related to Zn–S bonds. The bands at 3330 and 1627 cm^{-1} are associated with the constitutional water [29, 31]. Moreover, the bands located at 2047, 2048, and 2087 cm^{-1} are attributed to CO adsorption [30]. Considerable organic bands in the spectrum of the sample synthesized with the O:F ratio of 0.5 are due to incomplete removal of organic materials during the combustion process.

SEM micrographs of samples synthesized with different O:F ratios are shown in Fig. 4a–c. The products consist of highly agglomerated and semi-sintered particles. Because of the high value of exhausted gasses during the combustion process, all samples showed sponge-like morphologies. As illustrated in Fig. 4a, powders with mean particle size of 240 nm were obtained at O:F ratio of 1.

By increasing the fuel content (changing the O:F ratio from 1 to 0.66 and 0.5), the perfect combustion of the fuel with the air could not occur (see Fig. 1). Therefore, a gel-like

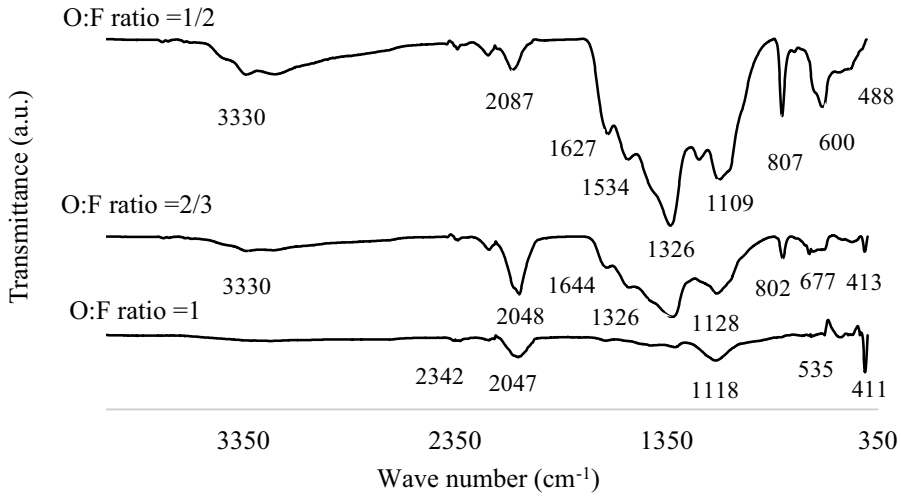

Fig. 3 FTIR spectra of samples synthesized with O:F ratios of 1, 2/3, and 1/2

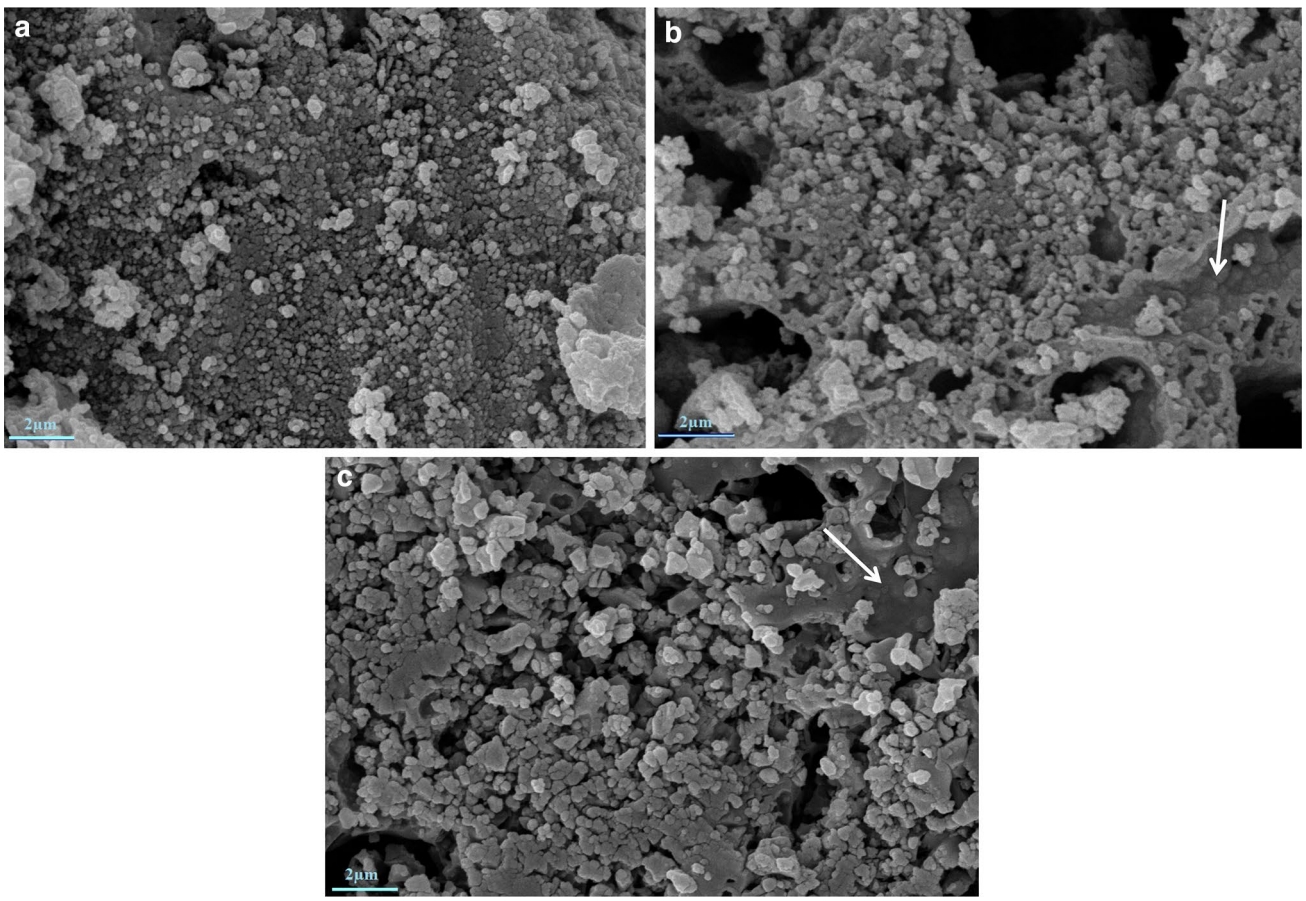

Fig. 4 SEM micrographs of samples synthesized with O:F ratios of **a** 1, **b** 2/3, and **c** 1/2. Gel-like product regions are specified by arrows

product was developed in some regions, as illustrated by arrows in Fig. 4b, c. Moreover, the mean particle size of the agglomerates increased considerably to 280 and 380 nm at O:F ratios of 0.66 and 0.5, respectively. It seems that by decreasing the O:F ratio, the ZnS clusters with higher agglomeration tendency were formed because of the their smaller size compared to ZnO crystals.

Figure 5a, b shows the PL spectra of the combustion products. There are two peaks at about 425–485 nm in the samples synthesized with O:F ratios of 0.66 and 1, as

illustrated in Fig. 5a. These peaks can be attributed to the recombination of photo-generated electron holes [31–34]. The strongest and the weakest peaks belong to the ZnS and ZnO, respectively, and are related to their band-gap energies [30–33]. The intensities of ZnS peaks are about 10% and 55% higher than ZnO ones for the samples synthesized with O:F ratios of 0.66 and 1, respectively.

The weaker peak of ZnS/ZnO nanocomposite, as compared with ZnS, indicates that coupling of ZnS with ZnO can effectively mitigate the recombination of photo-generated electron-hole pairs in ZnS [30–33]. There was a weak shoulder at about 530 nm which can be related to the deep-level defects (such as oxygen vacancies or interstitial Zn) in ZnO structure, and their recombination with holes generated by photons [35]. Therefore, the green emission at 530 nm was enhanced by developing the ZnO structure by increasing the O:F ratio from 0.5 up to 1. The spectrum of sample synthesized with O:F ratio of 0.5 showed somewhat different emission conditions (Fig. 5b). A broad peak with considerably higher intensity value (about four times) than other spectra can be observed. It seems that the incomplete combustion or the phase transformation from large ZnO to fine ZnS particles led to the formation of more crystalline defects and consequently, considerable increase in the PL value.

4 Conclusions

In the present study, ZnO/ZnS nanocomposites were synthesized by one-step solution combustion method using zinc nitrate and thiourea as starting materials. XRD results showed that thiourea could represent both functions of a combustion fuel and a sulphur source. Moreover, decreasing the O:F ratio led to incomplete reaction between Zn and O. Consequently, more ZnS was obtained in the final product due to the reaction of Zn and S. The final composites were not completely pure and contaminated by some unwanted organic compounds. Furthermore, microstructures of the

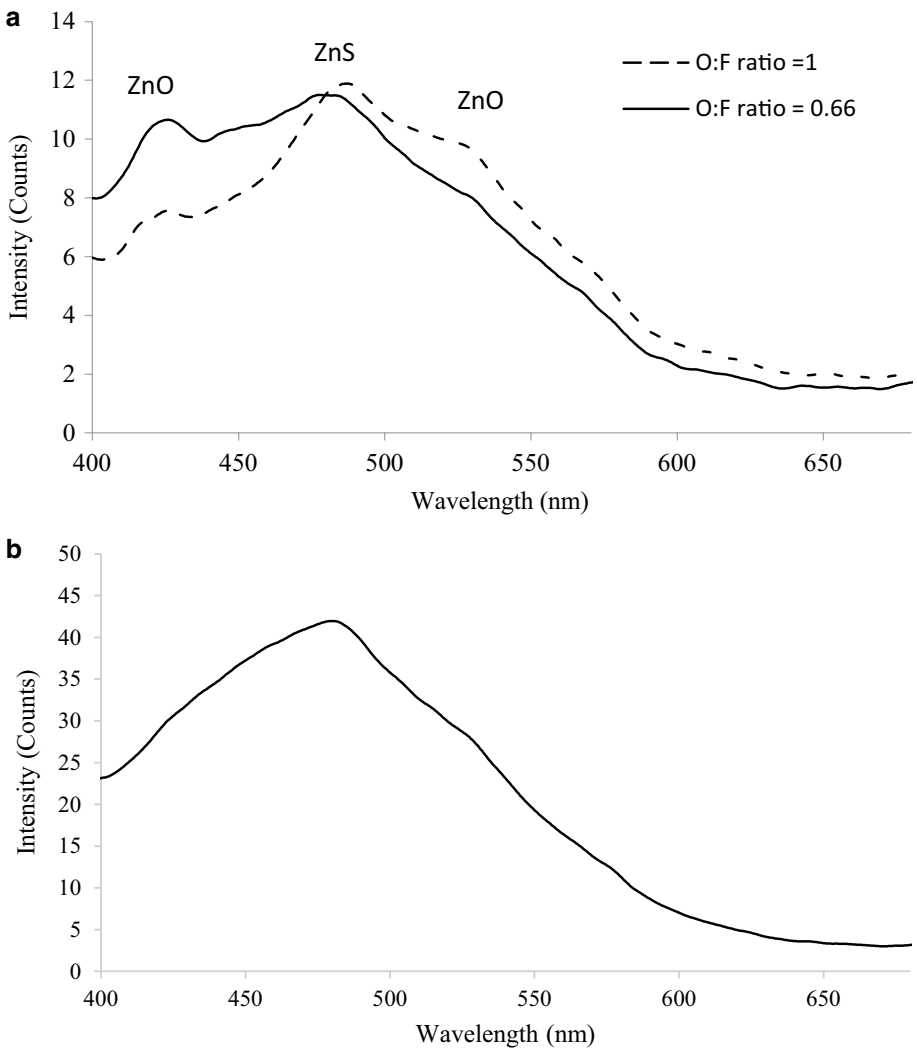

Fig. 5 PL spectra of samples synthesized with O:F ratios of **a** 1 and 2/3, and **b** 1/2

composites contained gel-like regions together with highly agglomerated nanoparticles. In addition, photoluminescence spectra demonstrated that samples synthesized with O:F ratio of 0.5 had more intensity due to more crystal defects and lower crystallinity.

Acknowledgements The authors acknowledge Amir Reza Gardeshzadeh for proofreading of the manuscript.

References

1. A. Salvador, M.C. Pascual-Marti, J.R. Adell, A. Requeni, J.G. March, Analytical methodologies for atomic spectrometric determination of metallic oxides in UV sunscreen creams. J. Pharm. Biomed. Anal. **22**, 301–306 (2002)
2. R. Li, S. Yabe, M. Yamashita, S. Momose, S. Yoshida, S. Yin, T. Sato, UV-shielding properties of zinc oxide-doped ceria fine powders derived via soft solution chemical routes. Mater. Chem. Phys. **75**, 39–44 (2002)
3. B.-C. Kim, J.-B. Paik, Y.-S. Han, N.-Y. Lee, B.-K. Lee. Synthesis of ZnO:Zn phosphors with reducing atmosphere and their luminescence properties. J. Korean Ceram. Soc. **37**(1), 1 (2000)
4. T. Tsuzuki, P.G. McCormick, ZnO nanoparticles synthesised by mechanochemical processing. Scr. Mater. **44**, 1731–1734 (2001)
5. N.L. Tarwal, P.S. Patil, Superhydrophobic and transparent ZnO thin films synthesized by spray pyrolysis technique. Appl. Surf. Sci. **256**, 7451–7456 (2010)
6. N.L. Tarwal, P.R. Jadhav, S.A. Vanalakar, S.S. Kalagi, R.C. Pawar, J.S. Shaikh, S.S. Mali, D.S. Dalavi, P.S. Shinde, P.S. Patil, Photoluminescence of zinc oxide nanopowder synthesized by a combustion method. Powder Technol. **208**, 185–188 (2011)
7. M. Xiying, S. Jingwei, Y. Zhangsen. The light emission properties of ZnS:Mn nanoparticles. Thin Solid Films **519**, 5043–5045 (2011)
8. B.S. Rema Devi, R. Raveendran, A.V. Vaidyan, Synthesis and characterization of Mn^{2+}-doped ZnS nanoparticles. Pramana **68**(4), 679–687 (2007)
9. H.C. Warad, S.C. Ghosh, B. Hemtanon, C. Thanachayanont, J. Dutta, Luminescent nanoparticles of Mn doped ZnS passivated with sodium hexametaphosphate. Sci. Technol. Adv. Mater. **6**, 296–301 (2005)
10. K. Manzoor, S.R. Vadera, N. Kumar, T.R.N. Kutty, Synthesis and photoluminescent properties of ZnS nanocrystals doped with copper and halogen. Mater. Chem. Phys. **82**, 718–725 (2003)
11. R. Viswanath, H.S. BhojyaNaik, G.S. Yashavanth Kumar, P.N. Prashanth, Kumar, EDTA-assisted hydrothermal synthesis, characterization and photoluminescent properties of Mn^{2+} doped ZnS. J. Lumin. **153**, 446–452 (2014)
12. E. Mohagheghpour, M. Rabiee, F. Moztarzadeh, M. Tahriri, M. Jafarbeglou, D. Bizari, H. Eslami, Controllable synthesis, characterization and optical properties of ZnS:Mn nanoparticles as a novel biosensor. Mater. Sci. Eng. C. **29**, 1842–1848 (2009)
13. R.H. Leach, C. Armstrong, J.F. Brown, M.J. Mackenzie, L. Randall, H.G. Smith. The Printing Ink Manual. Kluwer Academic, Dordrecht (1999)
14. X. Xu, L. Hu, N. Gao, S. Liu, S. Wageh, A.A. Al-Ghamdi, A. Alshahrie, X. Fang, Controlled growth from ZnS nanoparticles to ZnS–CdS nanoparticle hybrids with enhanced photoactivity. Adv. Funct. Mater. **25**, 445–454 (2015)
15. H. Zhao, Y. Dong, P. Jiang, X. Wu, R. Wu, Y. Chen, Facile preparation of a ZnS/ZnO nanocomposite for robust sunlight photocatalytic H_2 evolution from water. RSC. Adv. **5**, 6494–6500 (2015)
16. Ch Kim, S.J. Doh, S. Ge., S.J. Lee, H.Y. Kim, Visible-light absorptivity of a zincoxysulfide (ZnOxS1_x) composite semiconductor and its photocatalytic activities for degradation of organic pollutants under visible-light irradiation. Appl. Catal. A **330**, 127–133 (2007)
17. Q. Ma, Z. Wang, H. Jia, Y. Wang, ZnS–ZnO nanocomposites: synthesis, characterization and enhanced photocatatlytic performance. J. Mater. Sci. **27**, 10282–10288 (2016)
18. S.T. Aruna, S. Alexandera, Mukasyan. Combustion synthesis and nanomaterials. Curr. Opin. Solid State Mater. Sci. **12**, 44–50 (2008)
19. Ch. Binns. Introduction to Nanoscience and Nanotechnology. Wiley, Hoboken (2010)
20. R. Pozas, V.M. Orera, M. Oca˜na, Hydrothermal synthesis of co-doped willemite powderswith controlled particle size and shap. J. Eur. Ceram. Soc. **25**, 3165–3172 (2005)
21. K.C. Patil, Combustion synthesis: an update. Curr. Opin. Solid State Mater. Sci. **6**, 507–512 (2002)
22. F. Deganello, G. Marcì. Citrate–nitrate auto-combustion synthesis of perovskite-type nanopowders: a systematic approach. J. Eur. Ceram. Soc. **29**, 439–450 (2009)
23. E.M. Hunt, B. Keith, Nano-scale reactants in the self-propagating high-temperature synthesis of nickel aluminide. ActaMater. **52**, 3183–3191 (2004)
24. J. Liu, D. Zhang, X. Pu, J. Liu, R. Zhang, Combustion synthesis of $Zn_{1-x}Cd_xS$ and its photo degradation performance of methylene blue. Mater. Let. **117**, 158–161 (2014)
25. J.J. Kingsley, K.C. Patil, A novel combustion process for the synthesis of fine particle α-alumina and related oxide materials. Mater Let. **6**(11–12), 427–432 (1988)
26. W.H.R. Shaw, D.G. Walker, The decomposition of thiourea in water solutions. J. Am. Chem. Soc. **78**(22), 5769–5772 (1956)
27. V. Padmavathy, S. Sankar, V. Ponnuswamy, Influence of thiourea on the synthesis and characterization of chemically deposited nano structured zinc sulphide thin films. J. Mater. Sci. Mater. Electron. **29**, 7739–7749 (2018)
28. http://www.crct.polymtl.ca/reacweb.htm. Accessed Dec 2017
29. F. Gu, ShF. Wang, M. Kai Lu, G. Jun Zhou, D. Xu, D. Rong Yuan. Structure evaluation and highly enhanced luminescence of Dy^{3+}-doped ZnO nanocrystals by Li + doping via combustion method. Langmuir **20**, 3528–3531 (2004)
30. R.A.Nyquist,R.O.Kagel.Infrared Spectra of Inorganic Compounds ($3800–45cm^{-1}$).Academic Press, New York 1971.
31. C.F. Klingshirn, B.K. Meyer, A. Waag, A. Hoffmann, J. Geurts. Zinc Oxide from Fundamental Properties Towards Novel Applications. Springer, Heidelberg, 2010, pp. 77–94
32. P.A. RodnyiI, V. Khodyuk, Optical and luminescence properties of zinc oxide (Review). Opt. Spekctrok. **111**(5), 776–785 (2011)
33. H. Zeng, G. Duan, Y. Li, S. Yang, X. Xu, Blue luminescence of ZnO nanoparticles based on non-equilibrium processes: defect origins and emission controls. Adv. Funct. Mater. **20**(4), 561–572 (2010)
34. J. Ji, A.M. Colosimo, W. Anwand, L.A. Boatner, A. Wagner, P.S. Stepanov, T.T. Trinh, M.O. Liedke, R.T. Krause-Rehberg, E. Cowan, F.A. Selim, ZnO Luminescence and scintillation studied via photoexcitation, X-ray excitation, and gamma-induced positron spectroscopy. Sci. Rep. **6**, 31238 (2016)
35. M.J. Chithra, M. Sathya, K. Pushpanathan, Effect of pH on crystal size and photoluminescence property of ZnO nanoparticles prepared by chemical precipitation method. Acta Metall. Sin. (Engl. Lett.) **28**(3), 394–404 (2015)